COMBINED ANALYSIS OF HYPERSPECTRAL AND HIGH RESOLUTION IMAGE DATA IN AN OBJECT ORIENTED CLASSIFICATION APPROACH

A. Greiwe *, M. Ehlers

University of Osnabrueck, Research Centre for GIS and Remote Sensing (FZG), Germany
(ansgar.greiwe, manfred.ehlers)@uos.de

KEY WORDS: imaging spectroscopy, endmember selection, urban monitoring

ABSTRACT:

Many applications of remote sensing – like, for example, urban monitoring – require high resolution data for a correct determination of object geometry. These spatial high resolution image data contain often limited spectral information (e.g. three band RGB orthophotos). This poor spectral information lead often to classification errors between visible similar classes like water, dark pavements or dark rooftops. Additional information about the material of an urban object's surface is needed to separate these classes. Hyperspectral data with the typical high number of bands could be used to provide this information and allow a differentiation of material due to their typical spectra.

In the context of remotely sensed data, fusion is often performed by combining high spatial with high spectral resolution imagery on different levels. In contrast to pixel-based approaches like the IHS-transformation or PC spectral sharpening, the emphasis of this paper is fusion of data at feature level. Hyperspectral data recorded by the HyMap sensor are fused with high spatial resolution imagery (digital orthophotos) for a combined endmember selection and classification.

After a segmentation of the high spatial resolution orthophotos, the resulting segments will be used to detect those pixels in the hyperspectral data set , which represent candidates for the definition of reference spectra (so called endmember). Afterwards, the segments of the high spatial resolution data will be classified based upon the classification of the hyperspectral dataset and the application of overlay rules.

I. INTRODUCTION

Remote Sensing data used for spatial planning tasks require "high" resolution especially in urban areas. On the one hand, as a precondition for the detection of object shapes, high spatial resolution is necessary. On the other hand, high spectral resolution allows a differentiation of urban surfaces by their material composition due to their characteristic spectra.

However, high spatial resolution imaging sensors like the High Resolution Stereo Camera (HRSC-A) provide less than 10 bands to characterize the spectral feature of recorded data [1]. This low spectral resolution is insufficient to characterize the object's surface material by it's spectral characteristic (absorption bands, ratios). Hyperspectral sensors like the Digital Airborne Imaging Spectrometer (DAIS) or the Hyperspectral Image Mapper (HyMap) are able to record the reflecting spectra of an object's surface with 79 (DAIS) respective 128 (HyMap) bands [2, 3]. Due to technical limitations (e.g. sensors scan rate of 10 to 25 Hz) hyperspectral sensors are not able to deliver a spatial resolution of better than 2-3 m across flight track even at lower operating altitudes [4].

If an area of interest is recorded by both sensor types (maybe even co-registered), data fusion techniques are needed in order to retrieve the mutual benefit of both data types. In contrast to pixel based fusion algorithms [1, 5, 6] in this paper we discuss data fusion at feature level [7].

II. STUDY AREA AND DATA ACQUISITION

The study area is located in the centre of the City of Osnabrueck (Northwest Germany), covering 205x762 m^2 with different urban surface types:
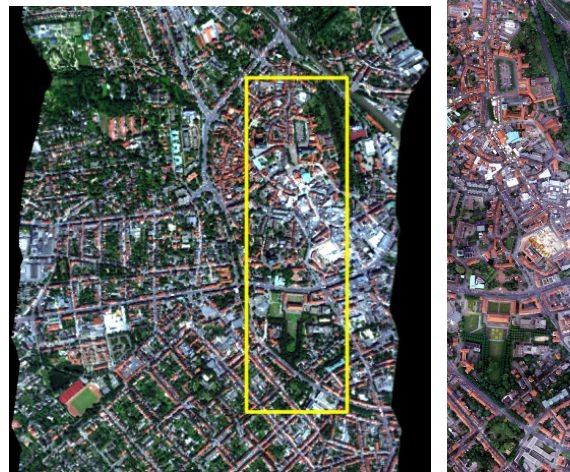

Figure 1. Study area of the city of Osnabrueck Left: Hyperspectral image data with study area (yellow box), Right: Corresponding high spatial resolution data

---

*   Ansgar Greiwe, FZG University of Osnabrueck, PO Box 1553, 49364 Vechta, Germany

For this study, different datasets were obtained for further investigations:

- Digital orthophoto data
- Digital elevation model (DEM) derived from cadastral data
- Digital surface model (DSM) derived from HRSC-A image data
- Hyperspectral image data

The hyperspectral data (Fig. 1 - left) were taken by the HyMap sensor. Scanned aerial images, taken by the Local Earth Observation System (LEO) [8] represent the image data of high spatial resolution (Fig. 1 - right).

A. Digital orthophoto system

The high spatial resolution data produced by LEO were 5.5cm x 5.5cm airphotos, taken on 16 May 2003 at an average flying height of 500 m. The image scale was about 1:10,000. The photos were scanned and resampled to a spatial ground resolution of 0.125 m. An orthoimage was generated using softcopy photogrammetry software with a resulting horizontal accuracy (one sigma) of $s_{x,y} = 0.2$ m. For further processing steps like image segmentation, the orthophoto was resampled by pixel aggregation to a resolution of 0.5 m (Fig. 2).

Figure 2. Orthophoto of the LEO system with overlay of a GIS layer (buildings).

B. Normalized Digital Surface Model

Information about the elevation of surfaces in the study area exist in two datasets:

- Digital elevation model (DEM, derived from cadastral data, grid size 12.5 m, vertical accuracy 0.5 m)
- Digital surface model (DSM, derived from HRSC-A image data, grid size 0.5 m, vertical accuracy 0.2 m)

For the generation of the DSM, a digital multiple correlation process is performed on the HRSC-A data [9]. The resulting DSM was normalized (nDSM) by use of the DEM data [10]. Unfortunately the HRSC-A campaign has been carried out in April 1999, an early stage of vegetation period. As a result the height of objects like trees or bushes could not be determined correctly. This effect is shown in Fig. 3, Trees in the middle of the image are displayed as a kind of flat terrain due to the erroneous DSM data. As a consequence the differentiation of vegetation objects in classes like "tree" and "lawn" has been left out in further processing.
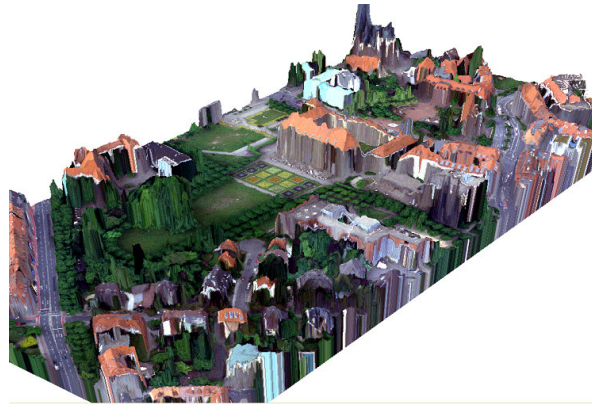

Figure 3. Orthophoto of the LEO draped over the DSM derived from HRSC-A data.

C. Hyperspectral image data

In 2003 the German Space Centre (DLR) in Oberpfaffenhofen coordinated a campaign on hyperspectral HyMap surveys in Europe (HyEurope2003). During this campaign, on July 15th, the hyperspectral image data were obtained by a north-south transect over the City of Osnabrueck.

The HyMap Sensor records 128 reflective bands covering the visible and near infrared range (VNIR) and the short wave infrared domain (SWIR) between 0.4 µm and 2.5 µm. With an operating altitude of 1500 m and a scan frequency of 16 Hz data could be recorded with a ground projected instantaneous field of view (GIFOV) of 3 m across and 4 m along flight track.

According to the whiskbroom principle of the opto-mechanical system of HyMap, the recorded lines of data were geocoded to a raster. This step was carried out by a parametric geocoding approach, implemented in the Software Package PARGE (implemented in IDL, executable in ENVI) [11]. To maximize the geometric accuracy during the orthorectification process, the nDSM with a grid size of 2 m was used. This oversampling (GIFOV = 3 m) reduced the amount of double-mapped image pixels from 1,8% to 0,3% (nDSM grid size 3 m vs. 2 m). The geometric accuracy of the image data was checked by cadastral GIS data (buildings) and estimated to be 1.8 m (one sigma).

Figure 4. RGB-Image of the HyMap data with overlay of a GIS-Layer (buildings).

After geometric processing the recorded radiances were corrected to absolute reflectances using the FLAASH software package (FLAASH = Fast Line-of sight Atmospheric Analysis of Hyperspectral Cubes) [12]. A subset of 104 bands was taken for further processing.

III. METHODOLOGY

Our methodological approach for data fusion is characterized by a object-oriented segmentation of the geometric high resolution orthophotos and a SAM-score generation of hyperspectral data. The method is based on a mutual support of both data types, in a segment based endmember selection, the geometric location of the pixel in hyperspectral data, which is representing an endmember of an urban surface type is determined by a segmentation of the high resolution image data. Pixel that are fully contained in a segment are candidates for the definition of reference spectra and are considered for the creation of a spectral library.

With the user-specific knowledge contained in that spectral libraries, the hyperspectral data are classified by the full pixel classification approach Spectral Angle Mapper (SAM). The classification results are transformed to an 8-bit *SAM-score* by a user-independent automated algorithm. Due to the identical geometric registration of both image data, the SAM-scores provide additional feature values for the image segments of the high geometric resolution orthophoto. The end product of this approach is a map produced by the classified segments. The workflow of our approach is shown in the following figure:
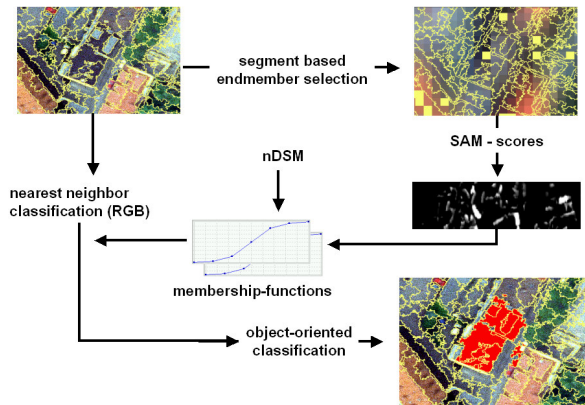

Figure 5. Segments of high resolution data (top left) are used for endmember selection in hyperspectral data (top right). Minimum distance (nearest neighbor) classification and score image are fused by using a linear membership function. Results are produced by a neural network classifier of eCognition.

A. Segment based endmember selection

Reference spectra for surface materials can be retrieved from field measurements or derived from image data. In case of a derivation of endmembers from image data, several algorithms have been developed:

- Manual endmember selection [13]
- Pixel Purity Index (PPI), implemented in ENVI [14]
- NFIND-R [15]
- Iterative Constrained Endmembers Algorithm (ICE) [16]
- Autonomous Morphological Endmember Extraction (AMEE) [17]

Urban surface endmembers are often a result of the mixture of manmade materials which usually leads to flat spectra. In addition, these endmembers have similar spectral features and

are hardly separable in feature space. As a consequence, automated algorithms like PPI or manual endmember selection lead to a significantly smaller number of defined urban surface endmembers. Due to this fact, the geometric location of pixels which represent endmembers are detected in our approach by segmentation of high spatial resolution data. The segments are generated by a multiresolution segmentation approach implemented in eCognition [18]. Only pixels of the hyperspectral data which are embedded in a N-8 neighborhood (Fig. 6) that is completely included in the identified image segments are considered for the manual definition of endmember spectra and stored in a spectral library (Fig. 6).
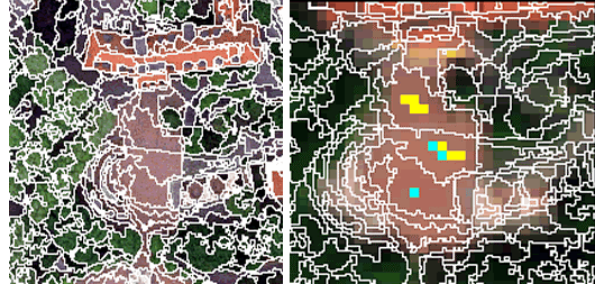

Figure 6. Segment based endmember selection. Left: high spatial resolution data and derived segments. Right: endmember candidates (yellow)
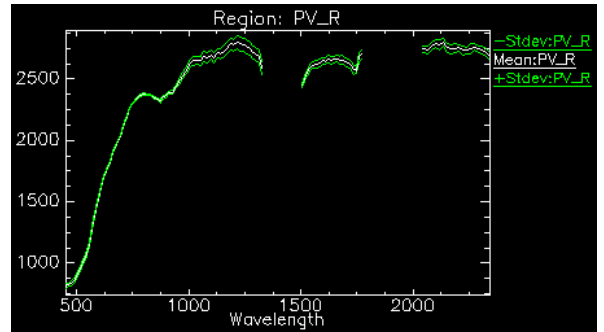

Figure 7. Retrieved endmember spectra of segment based selection process ("red pavement" from Fig. 6).

Using this approach for our study site, we were able to define one endmember for each a priori defined class.

B. SAM-score

For the further classification process a score for each pixel of the hyperspectral data has to be determined. The score is calculated by the results of the Spectral Angle Mapper (SAM). SAM calculates the cosine of a spectral angle for each given reference spectra with the following equation:

$$\cos\varphi = \frac{\sum_{i=0}^{n} e_i r_i}{\sqrt{\sum_{i=0}^{n} e_i^2}\sqrt{\sum_{i=0}^{n} r_i^2}} \tag{1}$$

where
- φ = spectral angle
- e = given image spectra
- r = reference spectra (endmember)
- n = number of classes

Beneath a class image, an additional result of SAM is a "rule image" which contains n spectral angles ($\varphi_{1...n}$, see eq. 1) for each image pixel at n given endmember. A value near zero in a rule image represents a good fit to a given endmember (Fig. 7, middle). In other words, a low value in layer n of the rule image indicate a candidate for the investigated class n.

Figure 8. SAM-score generation for class "dark red roof".

As shown in Fig. 8, dark red roof tiles in the orthophotos (Fig. 8 left) get a low value in the corresponding rule image after SAM classification (Fig. 8 middle). The SAM-score image (Fig. 8 right) is a kind of positive 8-bit greyscale image of the rule image data with a certain kind of sharpening. The transformation is done by the follow following equation:

$$ s_{c,i} = 255 \cdot \frac{\varphi_c^{max} - \varphi_i}{\varphi_c^{max} - \varphi_c^{min}} \quad with \, \varphi_c^{min} \leq \varphi_i \leq \varphi_c^{max} \quad (2) $$

where $s_{c,I}$ = *SAM*-score for Pixel i with respect to class c
   φ_i = spectral angle of investigated pixel
   φ_c^{max} = spectral angle which leads to a score of zero for class c (upper border)
   φ_c^{min} = best fitting spectral angle for class c which leads to a score of 255.
   n = number of classes

The sharpening effect of the transformation from rule image to SAM-score data (Fig. 8) depends on the thresholds given by the spectral angles φ_c^{max} and φ_c^{min} in (2). They have to be determined for each given endmember (rule image layer) and are highly depended on the spectral characteristics of the given endmember. These thresholds can be found by the following algorithm:

As a result of SAM the spectral angle values of one classified pixel are stored in a rule image. The spectral angles of one image pixel stored in that rule image could be treated as a vector. The order of the vector components is given by the order of the given endmembers in SAM. Sorting the vector components ascending (3), a new Vector is created so that the best fitting class for this pixel has the index i, the second best j and so on up to the worst fitting (largest spectral angle value) endmember n.

$$ W = \begin{bmatrix} \varphi_i \\ \varphi_j \\ ... \\ \varphi_n \end{bmatrix} \quad \text{with } \mathbf{n} = \text{number of endmember} \quad (3) $$

The above mentioned thresholds φ_c^{max} and φ_c^{min} for every class c have to be estimated by finding the "worst" spectral angle.

Defining the following constraints, every pixel is scanned:

1) If the spectral angle of the best fitting class i is significant smaller than the second best class j ($|\varphi_j - \varphi_i| > 0.33 \, \varphi_i$), this pixel is marked as candidate for a SAM-score of class i. (No other class spectra matches better to this pixel than the endmember of class i).
2) If the second or even third best spectral angle (classes j,k) are near the best fitting angle ($|\varphi_{j,k} - \varphi_i| < 0.33 \varphi_i$) the Pixel is also marked as a candidate for class j or k.

After marking the pixels under these constraints, for any given class c all corresponding marked pixels are used to estimate the smallest (φ_c^{min}) respectively the largest (φ_c^{max}) spectral angle. Using (2), the transformation of any given spectral angle to the SAM-scores is now possible as shown in the following figure:
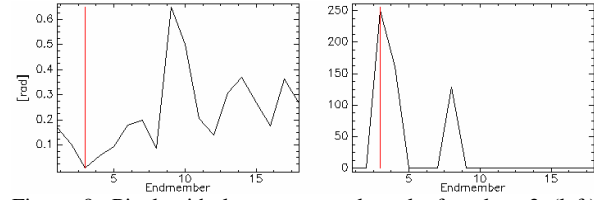

Figure 9. Pixel with lowest spectral angle for class 3 (left) receives highest SAM-score for this class but also a score for classes 4 and 8.

C. Classification of image objects

Beneath the information about the average height of a segment and the RGB values from the orthophotos the above described SAM-scores could be used as an additional feature information. Like a DSM, the 8-bit SAM-score is also stored in a greyscale image and averaged by overlay operation in a GIS. As a result, for each given class, a SAM-score is available (Fig. 10.).
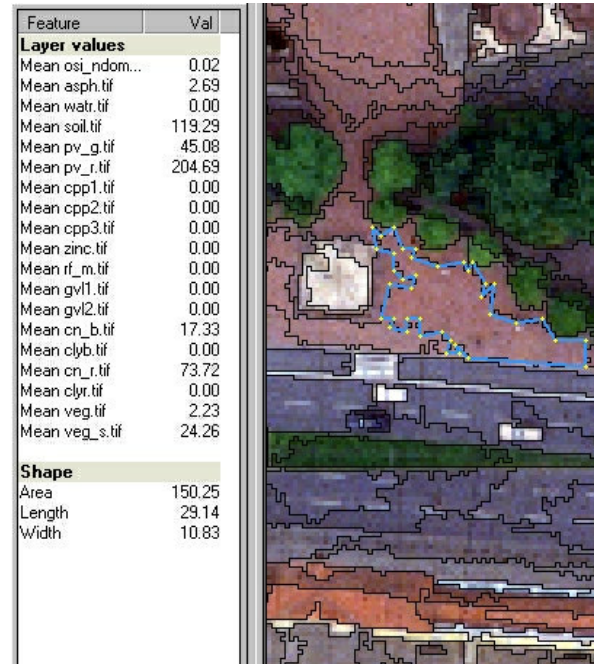

Figure 10. SAM-scores for a segment

The creation of image objects (segments) and the final classification is performed within the software eCognition. eCognition provides a neural network classifier which allows the user to create feature specific membership functions considering the SAM-scores. The segment displayed in Fig. 10 has a SAM-score of 204.69 for the class "red pavement" and a SAM-score of 73.73 for "red concrete" which has similar spectral features. Due to the high SAM-score of the material "red pavement" and the average height of 0.02 m ("osi_ndom" - value) this segment is classified as "red pavement".

IV. RESULTS

19 different, visibly similar classes have been defined with a differentiation in material classes in order to prove the methodology. For example, red roof tops were divided into "red roof concrete" and "red roof clay". Three different classification scenarios were defined to investigate the performance of the presented approach. A minimum distance classification applied on the RGB feature space of the orthophoto (RGB), an additionally combination with the segment's elevation and at last the implementation of SAM-scores into the classification process.
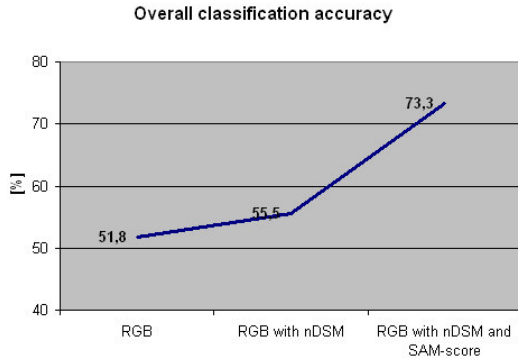

Figure 11. Increasing overall classification accuracy

For each of the classification scenarios the overall accuracy was estimated. The relative low overall accuracy of the RGB scenario could be explained by the strong similarities of the defined classes.
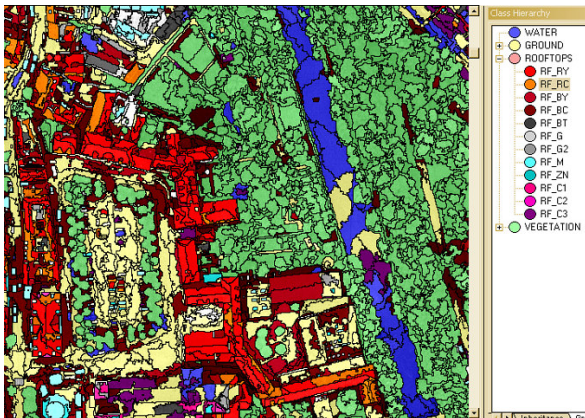

Figure 12. Classification Scenario "RGB" of Fig. 2

The improvement of nearly 20% in classification accuracy shows, however the benefit of an integration of hyperspectral image data into the classification process of surfaces with similar features but different material.
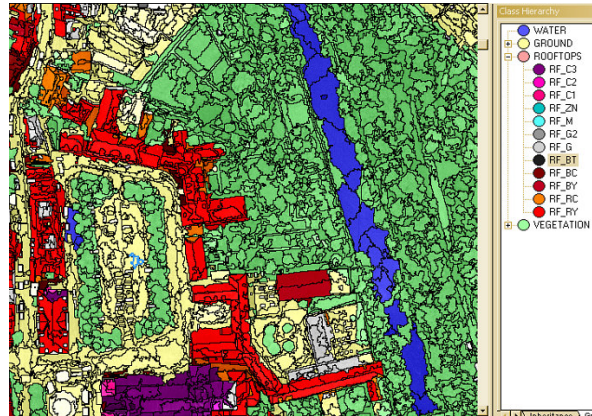

Figure 13. Classification Scenario "RGB with nDSM and SAM-score"

V. CONCLUSION

The presented approach uses the benefits of a combination of high spatial and high spectral resolution remote sensing data. It could be proved that a segment based endmember selection results in a suitable spectral library. With an automated SAM-score generation, additional feature values for the image segments could be generated. The additional inclusion of hyperspectral image data into a classification process of high spatial resolution image data show significant improvements and allow material differentiation of urban surfaces.

The accuracy of the presented approach is highly dependent on the geometric correctness of the acquired image data. The results are based on image data that are not co-registered. Future co-registered sensor combinations like ARES [19] and HRSC will show if the overall accuracy can be increased.

REFERENCES

[1] F. Lehmann, T. Bucher, S. Hese, A. Hoffmann, S. Mayer, F. Oschtüz, and Y. Zhang, "Die Kombination von hyperspektralen HyMap-Daten und HRSC-A Multispektral und DGMdaten zur Validierung und Nutzung in verschiedenen Anwendungsgebieten," in DGPF Jahrestagung, 1998.

[2] P. Strobl, R. Richter, F. Lehmann, A. Müller, B. Zhukov, and D. Oertel, "Dais system performance, first results from the 1995 evaluation campaigns," in Second International Airborne Remote Sensing Conference and Exhibition, Vol. II, ERIM, Environmental Research Institute of Michigan, ed., pp. 325–334, San Francisco, California, 1996.

[3] T. Cocks, R. Jenssen, A. Stewart, I. Wilson, and T. Shields, "The hymap airborne hyperspektral sensor: The system, calibration and performance," Proc. of 1. EARSEL Workshop on Imaging Spectroscopy, Zurich, 1998.

[4] I. J. Wilson and T. D. Cocks, "Development of the Airborne Reflective Emissive Spectrometer (ARES) - a Progress Report," in Proc. of 3rd EARSeL Workshop on Imaging Spectroscopy 13 - 16 May 2003, M. Habermeyer, A. Müller, and S. Holzwarth, eds., pp. 50–55, 2003.

[5] B. Zhukov, D. Oertel, and F. Lanzl, "Unmixing and Fusion of Multi-Resolution Images with Applications to TM/Landsat and Simulated ASTER Data," in Proceedings of the Second International Conference "Fusion of Earth Data - Merging Point Measurements, Raster Maps and Remotely Sensed Images", T. Ranchin and L. Wald, eds., 1998.

[6] B. Zhukov, D. Oertel, F. Lanzl, and G. Reinhäckel, "Unmixing-based multisensor multiresolution image fusion," IEEE Transactions on Geoscience and Remote Sensing 37(3), pp. 1212–1225, 1999.

[7] C. Pohl and J. v. Genderen, "Multisensor image fusion in remote sensing: concepts, methods and applications," Int. J. Remote Sensing 19, pp. 823–854, 1998.

[8] M. Bäumker and F.-J. Heimes, "New calibration and computing method for direct georeferencing of image and scanner data using the position and angular data of an hybrid navigation system," in Integrated Sensor Orientation, Proceedings OEEPE-Workshop, Hannover, 2001.

[9] G. Neukum and HRSC-Team, "The Airborne HRSC-AX Cameras: Evaluation of the Technical Concept and Presentation of Application Results after One Year of Operation," in Photogrammetric Week 2001, D. Fritsch and R. Spiller, eds., pp. 117–130, Wichmann Verlag, Heidelberg, 2001.

[10] M. Möller, Urbanes Umweltmonitoring mit digitalen Flugzeugscannerdaten, Wichmann Verlag, Heidelberg, 2003.

[11] D. Schläpfer, M. Schaepman, and K. Itten, "Parge: Parametric geocoding based on gcp-calibrated auxiliary data," Proc. SPIE Vol. 3438, Imaging Spectrometry IV, pp. 334–344, San Diego, 1998.

[12] S. M. Adler-Golden, M. W. Matthew, L. S. Bernstein, R. Y. Levine, A. Berk, S. C. Richtsmeier, P. K. Acharya, G. P. Anderson, G. Felde, J. Gardner, M. Hike, L. S. Jeong, B. Pukall, J. Mello, A. Ratkowski, and H. H. Burke, "Atmospheric correction for short-wave spectral imagery based on modtran4," in Imaging Spectrometry, SPIE Proceedings(3753), pp. 61–69, 1999.

[13] Bateson and Curtiss, "A Method for manual endmember Selection and Spectral Unmixing," Remote Sensing and Environment (55), pp. 229–243, 1996.

[14] J. W. Boardman, F. A. Kruse, and R. O. Green, "Mapping target signatures via partial unmixing of aviris data," Summaries, Fifth JPL Airborne Earth Science Workshop, JPL Publication 95-1 (1), pp. 23–26, 1995.

[15] M. E. Winter, "Fast autonomous spectral endmember determination in hyperspectral data," Proceedings of the Thirteenth International Conference on Applied Geologic Remote Sensing (II), pp. 337 – 344, 1999.

[16] M. Berman, H. Kiiveri, R. Lagerstrom, A. Ernst, R. Dunne, and J. Huntington, "Ice: An automated statistical approach to identifying endmembers," in IEEE International Geoscience and Remote Sensing Symposium, Toulouse, France, IEEE Proceedings (Vol. 1), pp. 279–283, 2003.

[17] A. Plaza, P.Martinez, R. Perez, and J. Plaza, "Spatial / spectral endmember extraction by multidimensional morphological operations," IEEE Transactions on Geoscience and Remote Sensing 40(9), pp. 2025–2041, 2002.

[18] M. Baatz and A. Schäpe, "Multiresolution segmentation - an optimized approach for high quality multiscale image segmentation," in AGIT XIII, Strobl, Blaschke, and Griesebner, eds., Wichmann, Heidelberg, 2000.

[19] H. Kaufmann, S. Chabrillat, D. S., M. Habermeyer, S. Holzwarth, H. Mehl, A. Müller, R. Richter, and K. Segl, "Environmental Mapping and Analysis Program Based on the Use of the Airborne Reflective Emissive Spectrometer (ARES)," in Proc. of 3rd EARSeL Workshop on Imaging Spectroscopy 13 – 16 May 2003, M. Habermeyer, A. Müller, and S. Holzwarth, eds., pp. 15–24, 2003.